文章编号 2095-1531(2018)04-0590-14

Design and fabrication of 12 W high power and high reliability 915 nm semiconductor lasers

QIU Bo-cang[1,2,3*], MARTIN Hai HU[1,2,3], WANG Wei-min[2], LIU Wen-bin[2], BAI Xue[2]
(1. *Research Institute of Tsinghua University in Shenzhen, Shenzhen* 518057, *China*;
2. *Shenzhen Raybow Optoelectronics Corp, Shenzhen* 518055, *China*;
3. *Guangdong Provincial Key Laboratory of Optomechatronics, Shenzhen* 518057, *China*)
* *Corresponding author, E-mail: qiubocang@raybowlaser.com*

Abstract: In this paper, a high efficiency and high reliability 915 nm semiconductor laser is designed and fabricated, which is a key component of the fiber lasers. In order to maximize the electro-optic conversion efficiency of the device, a double asymmetric large-cavity waveguide structure is adopted in the design, and the quantum well structure, waveguide structure, doping, and device structure are systematically optimized. Device simulations show that the device's maximum electro-optical conversion efficiency reaches 67% at an ambient temperature of 25 ℃. The material is grown by Metal Organic Chemical Vapor Deposition(MOCVD), and a laser chip having a light emitting region width of 95 μm and a cavity length of 4.8 mm is prepared. Tests show that the efficiency of the packaged device and other parameter indices have reached the advanced level of similar devices in the world. In the case that the threshold current is 1 A at room temperature, the slope efficiency is 1.18 W/A, the maximum electro-optic conversion efficiency is 66.5%, the output power is 12 W, and the electro-optical conversion efficiency reaches 64.3%. It can be seen that the test results are in good agreement with that of the device theory simulation. After approximately 6 000 hours of long-life accelerated testing, the device power does not attenuate, indicating that the produced high-power 915 nm laser chip has very high reliability.

Key words: semiconductor laser; electro-optical conversion efficiency; brightness; cavity surface catastrophic power

收稿日期:2017-12-25;**修订日期**:2018-02-12

基金项目:国家高技术研究发展计划(863 计划)(No. 2015AA016901);广东省引进创新科研团队项目(No. 2011D040);深圳市孔雀计划项目(No. KQTD201106)

Supported by National High Technology Research and Development Program of China(No. 2015AA016901); Innovative R&D Team Leadership of Guangdong Province Program(No. 2011D040); Shenzhen City Peacock Program(No. KQTD201106)

12 W 高功率高可靠性 915 nm 半导体激光器设计与制作

仇伯仓[1,2,3*],胡　海[1,2,3],汪卫敏[2],刘文斌[2],白　雪[2]
(1. 深圳清华大学研究院,广东 深圳 518057;
2. 深圳瑞波光电子有限公司,广东 深圳 518055;
3. 广东省光机电一体化重点实验室,广东 深圳 518057)

摘要:本文设计并制作了一种高效率、高可靠性的 915 nm 半导体激光器。半导体激光器是光纤激光器的关键部件,为了最大限度地提高器件的电光转换效率,在设计上采用双非对称大光腔波导结构,同时对量子阱结构、波导结构、掺杂以及器件结构进行了系统优化。器件模拟表明,在 25 ℃环境温度下,器件的最高电光转换效率达到 67%。采用金属有机气相沉积(MOCVD)法进行材料生长,随后制备了发光区域宽度为 95 μm、腔长为 4.8 mm 的激光芯片。测试表明,封装后器件的效率以及其它参数指标达到国际先进水平,在室温下阈值电流为 1 A,斜率效率为 1.18 W/A,最高电光转换效率达 66.5%,输出功率 12 W 时,电光转换效率达到 64.3%,测试结果与器件理论模拟高度吻合。经过约 6 000 h 的寿命加速测试,器件功率没有出现衰减,表明制作的高功率 915 nm 激光芯片具有很高的可靠性。

关　键　词:半导体激光器;电光转换效率;亮度;腔面灾变功率
中图分类号:TN248.4　　**文献标识码**:A　　doi:10.3788/CO.20181104.0590

1　Introduction
引　言

The performance of ytterbium-doped fiber laser (YDFL) has improved dramatically over the past 20 years and its output power has increased at an average rate of 170% per year. In 2009, Stile reported that IPG used large-mode single-mode fiber (large mode area:LMA) by IPG to obtain 10 000 watts of output power[1]. Due to the outstanding characteristics of fiber lasers, including output power, beam quality, easy system integration with industrial equipment systems, laser industrial processing equipment with fiber lasers as its core components has been widely used in various industrial manufacturing processes[2-3]. YDFL has a very broad absorption spectrum (approximately 900 – 977 nm), and its pump source wavelength is usually set at about 915 nm[4]. Although high-power 915 nm semiconductor lasers are quite mature, industrial and academic circles are still working hard to continuously improve the parameters and the performance of the devices, including beam quality, polarization characteristics, output power, and electro-optical conversion efficiency[5]. Murita *et al*. from Hamamatsu Photonics Japan reported high-electron-to-optical conversion efficiency of 976 nm (96 μm) laser in 2013. The device has a maximum electro-optic conversion efficiency of 68% (corresponding to an output power of 6.3 W) at a test environment of 20 ℃, and the efficiency is reduced to 61% at an output power of 15 W[6]. Crump et al. from FBI Research Institute Germany reported that the 96 μm-wide laser had a lifetime test of more than 4 000 hours at 20 W output power[7]. Literature[8-9] reported that the efficiency of a 976 nm device at room temperature at 10 W output power reached 65%. In addition to output power and efficiency, device reliability is also a very important design consideration. Although the reliability of the device is related to many factors, including junction temperature, current density, and optical power density, the optical power density has a more direct effect on the reliability of the device, especially the reliability related to the facet failure. In order to improve the reliability of the device operation, several methods are used, such as low power

density design[10], non-absorption window facet technology[11]. In this paper, for the requirements of high power and high electro-optic conversion efficiency and high reliability, we adopt the design concept of double asymmetric large optical cavity[7,12-13] and that of low power density, and systematically optimize the device's material structure, including the waveguide structure, doping profile, device cavity length, facet reflectance, *etc*. to improve the device efficiency. Tests have shown that a device with a width of 95 μm and a cavity length of 4.8 mm can reliably operate at 12 W with a threshold current of approximately 1 A, a slope efficiency of 1.18 W/A. When the output power is 12 W, the corresponding electro-optic conversion efficiency is 64.3%, while the highest conversion efficiency is 66.5% (corresponding to 8.9 W of output power). The device's energy conversion efficiency and other major parameter levels have reached the level of international devices of the same type.

掺有稀土元素镱的光纤激光器(YDFL)性能在过去20余年来取得了惊人的提升,其输出功率的提升速率平均每年达到170%,2009年,Stile报告了IPG公司采用大模场单模光纤(large mode area,LMA)获得了一万瓦的输出功率[1]。由于光纤激光的优异特性,包括:输出功率、光束质量、易于和工业设备系统进行系统集成,以光纤激光器为其核心部件的激光工业加工设备已经大规模应用于各种工业制造过程中[2-3]。YDFL的吸收谱极为宽广(大约900~977 nm),其泵浦源的波长通常选在915 nm左右[4]。虽然高功率915 nm半导体激光已经相当成熟,然而工业与学术界仍在不断努力,以期持续改进器件的参数性能指标,包括:光束质量、偏振特性、输出功率以及电光转换效率等[5]。2013年,日本Hamamatsu Photonics公司的Morita等人报导了高电光转换效率的976 nm宽条(96 μm)激光,器件在20℃测试环境下,最大电光转换效率为68%(对应于输出功率6.3 W),在输出功率为15 W时,效率降低到61%[6]。2009年,德国FBI研究所的Crump等人报导了96 μm条宽的激光器在20 W输出功率时寿命测试超过4 000 h[7]。文献[8-9]报导了976 nm器件在室温下10 W输出功率时效率达到65%。除了输出功率与效率,器件的可靠性也是非常重要的设计考虑。尽管器件的可靠性与多种因素有关,包括结温、电流密度以及光功率密度等,但光功率密度对器件的可靠性特别是与腔面失效有关的可靠性影响更为直接。为了改善器件运行的可靠性,人们采用若干方法,如低功率密度设计[10]、无吸收腔面技术等[11]。针对高功率以及高电光转换效率以及高可靠性这一要求,本文采用了双非对称大光腔结构[7,12-13]、低功率密度设计理念,并系统地优化了器件的材料结构,包括波导结构、掺杂分布、器件腔长、腔面反射率等来提高器件效率。实验测试表明,95 μm条宽、4.8 mm腔长的器件可以可靠地工作在12 W,阈值电流大约为1 A,斜率效率为1.18 W/A,输出功率为12 W时所对应的电光转换效率为64.3%,而最高转换效率则为66.5%(对应于输出功率8.9 W)。器件的能量转换效率以及其它主要参数水平达到了国际同类器件的水平。

2 Epitaxial structure design
外延结构设计

Semiconductor epitaxial structure design involves the selection of quantum wells, waveguide design, and doping optimization. For 915-nm lasers, the quantum wells can use 5 – 8 nm compressive strain material In(x)GaAs, and the content of In component needs to be adjusted according to the thickness of the used quantum well to ensure that the lasing wavelength is around 915 nm. In addition to the quantum well material, the height of the barrier has a significant influence on the performance of the device because the barrier height affects the internal quantum efficiency and temperature characteristics of the device. In order to examine the exact relationship between the barrier height and the quantum efficiency within the device, a numerical model of internal quantum efficiency based on traveling wave amplification is developed. This model considers the photon flux density at different locations in the resonator, the carrier concentration in the quantum wells, thermionic emission, *etc*., to calculate the number of radiatively recombined carriers among. Fig. 1 shows the relationship between the internal

quantum efficiency and the barrier Al content based on our traveling wave amplification model. It can be found from the calculation that for the 915 nm high-power laser, the internal quantum efficiency reaches 99% when the content of the Al component in the Al(x)GaAs material exceeds 0.23. Based on the above calculation, the quantum well structure we selected is $In_{0.10}GaAs/Al_{0.23}GaAs$.

半导体外延结构设计涉及到量子阱的选取、波导设计以及掺杂优化等。对于 915 nm 激光来说,量子阱可选用 5 ~ 8 nm 的压应变材料 In(x)GaAs材料,其中 In 组份含量需要根据所采用的量子阱厚度做必要的调整,以保证激射波长为915 nm 左右。除量子阱材料外,势垒的高度对器件的性能影响至关重要,因为势垒高度影响器件的内量子效率以及温度特性。为了考察势垒高度与器件内量子效率之间的精确关系,我们发展出一种基于行波放大的内量子效率计算模型,模型中考虑了在谐振腔中不同位置的光子通量密度、量子阱内的载流子浓度、热电子发射等,从而计算出受激复合的载流子占注入载流子的比例。该计算模型是我们自己首次提出的一种计算方法,尚未查阅到类似的文献。图 1 是根据我们的行波放大模型计算的内量子效率与势垒 Al 组份含量之间的关系。由计算可见,对于915 nm 高功率激光来说,当 Al(x)GaAs 材料中 Al 组份含量超过 0.23 时,内量子效率达到 99%。基于上述计算,我们选取的量子阱结构为 $In_{0.10}GaAs/Al_{0.23}GaAs$。

After the quantum well material is determined, the material structure design should be performed according to actual application requirements, and its main purpose is to find a waveguide structure that satisfies the laser operating parameters (such as a suitable quantum well confinement factor). This is because the material structure of the semiconductor laser is essentially a typical one-dimensional waveguide structure, *i. e.*, a low refractive index under clad layer, a high refractive index waveguide core, and a low refractive index upper cladding layer in the material growth direction in turn. In this way, light waves can be transmitted in a guided wave manner in the growth plane. The waveguide structure generally has two different design ideas: one is a traditional narrow-waveguide single-mode design[10,14], and the other is a popular large-cavity structure design in high-power lasers. The advantage of the large-cavity structure is that the optical loss can be designed to be very low because of the small overlap of the light field and the material doped region, so that free carrier absorption (FCA)[15] and inter-valence band absorption (IVBA)[16] can be minimized. The waveguide design calculates the mode field distribution of light in the waveguide in the vertical direction (*i. e.*, growth direction) according to the refractive index distribution of the given epitaxial structure. Then, the parameters related to the device performance including the quantum well confinement factor Γ, far field distribution, normalized power density, *etc.* are calculated by the mode field distribution. The mode field distribution in the optical waveguide needs to solve the following Helmholtz equation derived from the Maxwell electromagnetic equations:

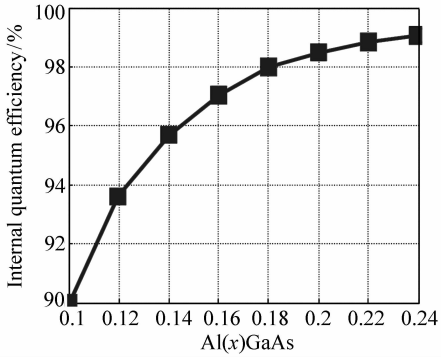

Fig. 1　Relationship between internal quantum efficiency and Al component content of quantum well barrier materials

图 1　内量子效率与量子阱势垒材料 Al 组份含量之间的关系

量子阱材料确定后,需要根据实际应用需求进行材料结构设计,其主要目的是找出满足激光工作参数(如合适的量子阱限制因子)的波导结构。这是因为半导体激光器的材料结构本质上是一典型的一维波导结构,即在材料生长方向上,先后是低折射率的下包层,高折射率的波导核以及

低折射率的上包层。这样光波可以在生长面内以导波的方式进行传播。波导结构一般有两种不同的设计思路:其一为传统的窄波导单模设计[10,14],其二是在高功率激光中颇为流行的大光腔结构设计。大光腔结构的优点是光损耗可以被设计得非常低,因为光场和材料掺杂区域重叠很小,如此一来,自由载流子吸收(FCA)[15]以及价带间的空穴跃迁引起的吸收(IVBA)[16]可以被降低到最小程度。波导设计是根据给定的外延结构的折射率分布计算光在波导中垂直方向(亦即生长方向)的模场分布,然后通过模场分布计算出与器件性能相关的参数包括量子阱限制因子 Γ、远场分布、归一化的功率密度等。光波导中的模场分布需要求解从麦克斯韦尔电磁方程组推导而来的下述亥尔姆霍尔兹方程:

$$\frac{\mathrm{d}^2E}{\mathrm{d}x^2} = -K_0^2[n(x)^2 - n_e^2]E \ , \qquad (1)$$

This equation is actually an eigenvalue equation, which means that the effective refractive index of the waveguide mode can only take a specific discrete value, and each eigenvalue (effective refractive index value) corresponds to a mode field distribution. For a single mode waveguide, only the fundamental mode exists, and correspondingly, there are multiple waveguide modes for the multimode waveguide.

这一方程式实际上是一本征值方程,意味着波导模式的有效折射率只能取特定的分立值,每一个本征值(有效折射率值)对应一个模场分布。对于单模波导来说,只存在基模,与此相对应,多模波导存在多个波导模式。

In equation (1), represents the electric field strength of light waves, $K_0 = \frac{2\pi}{\lambda_0}$ (λ_0 is wavelength in vacuum) is the free space wave number, $n(x)$ is the refractive index distribution of the epitaxial structure in the growth direction, and the refractive index distribution of the material depends on the change of the material composition in the growth direction. Fig. 5 shows the refractive index changes along the growth direction of the material structure designed in this paper, the dispersion relationship of AlGaAs materials refer to [12], and n_e is the effective refractive index of the desired waveguide mode. The mode field distribution within the waveguide can be calculated using the transfer matrix method (TMM). In order to calculate the mode gain, considering that the mode field distribution is only partially overlapping with the active region, the concept of the quantum well confinement factor has been introduced. The quantum well confinement factor Γ is defined as the ratio of the distribution of the light field intensity of the waveguide mode (proportional to E^2) at the quantum well to the total area distribution, *i. e.*:

方程式(1)中,E 表述光波的电场强度,$K_0 = \frac{2\pi}{\lambda_0}$,($\lambda_0$ 为真空中的波长)是自由空间波数,$n(x)$ 是外延结构在生长方向上的折射率分布,而材料的折射率分布取决于生长方向上的材料组份变化(图5给出了本文设计的材料结构沿生长方向上的折射率变化,AlGaAs 材料的色散关系参见文献[12]),n_e 是所求的波导模式的有效折射率。波导内的模场分布可非常容易地用转移矩阵法(TMM)进行计算。考虑到模场分布与有源区只是部分重叠,为了计算模式增益,人们引入了量子阱限制因子这一概念。量子阱限制因子 Γ 被定义为波导模式的光场强度(正比于 E^2)在量子阱处的分布占整个区域分布的比例,即:

$$\Gamma = \frac{\int_{\mathrm{QW}} E^2\mathrm{d}x}{\int_{\mathrm{all}} E^2\mathrm{d}x} \ , \qquad (2)$$

The threshold current of chip can be expressed as:

而芯片的阈值电流可以表示为:

$$I = e(AN_{\mathrm{th}} + BN_{\mathrm{th}}^2 + CN_{\mathrm{th}}^3)dwL/\eta \ , \qquad (3)$$

Where N_{th} is the carrier concentration in the quantum well when the threshold condition is reached, e is the electron charge amount; A, B, C are non-radiative recombination coefficient, spontaneous emission coefficient, and Auger recombination coefficient, respectively. By comparing with a large number of experimental test data, we fit the A, B, C coefficient values at 915 nm to approximately $5 \times 10^{-7}\ \mathrm{s}^{-1}$, $7 \times 10^{-10}\ \mathrm{cm}^3/\mathrm{s}$, $1 \times 10^{-30}\ \mathrm{cm}^6/\mathrm{s}$, re-

spectively. d, w, L are the quantum well thickness, the width of the chip current injection region, and the cavity length, respectively, and η is the carrier quantum well implantation efficiency, which can be further expressed as $\eta = 1 - \eta_e$, η_e is the probability that carriers escape the quantum well. The following equation solves A in equation (3):

式中,N_{th}为到达阈值条件时量子阱内的载流子浓度,e 为电子电荷量,A、B、C 分别为非辐射复合、自发辐射以及俄歇复合系数。通过与大量实验测试数据比较,我们拟合出 915 nm 时的 A、B、C 系数取值分别大约为 5×10^{-7} s^{-1}、7×10^{-10} cm^3/s、1×10^{-30} cm^6/s。d、w、L 分别为量子阱厚度、芯片电流注入区宽度以及腔长,η 为载流子的量子阱注入效率,可以进一步表示为 $\eta = 1 - \eta_e$,η_e 为载流子逃逸出量子阱的几率。式(3)中的 N_{th}需要求解下方程:

$$\Gamma g(N_{th}) = \alpha - \ln(R_A R_H)/(2L). \quad (4)$$

Equation (4) describes the device reaching the threshold condition when the gain and loss obtained are balanced and the photons go back and forth within the cavity, where $g(N_{th})$ is the material gain of the quantum well. The calculation can be referred to Ref. [17]. α is the cavity loss, R_A and R_H are the reflectivity of the two facets. The left side of equation (4) is the mode gain of the light, and the first term on the right side of the equation is the internal loss(we will then see the dependence of the loss on material doping). The second term is loss related to the mirror loss.

方程(4)意味着当光子在腔内往返一周时所获得的增益与损耗达到平衡时,器件达到阈值条件,式中,$g(N_{th})$是量子阱的材料增益,其计算可以参考文献[17],α 为腔内光损耗,R_A、R_H分别为两个腔面镀膜的反射率。式(4)等式左边为光的模式增益,而等式右边第一项为腔内光损耗(随后我们将会看到损耗与材料掺杂之间的依赖关系),第二项为与腔面透光有关的损耗。

The divergence angle of the beam, that is, the far field distribution and the near field distribution constitute a Fourier transform, and it is also necessary to consider the refraction of light at the interface between the semiconductor and the air. Fig. 2 – Fig. 4 shows the relationship among quantum well confinement factor, beam divergence angle (full width at half maximum(FWHM)), normalized power density and the total waveguide thickness(the total thickness of the SCH layer) in the case of symmetric waveguides where the aluminum component of the waveguide layer is 0.06, 0.09, and 0.12 respectively higher than the aluminum component of the cladding layer. In this paper, the normalized power density refers to the peak power density corresponding to a 100 μm wide active area chip output power of 10 W. It can be seen from the figure that all three parameters obtain the highest value at a certain SCH thickness and after the highest point, the above parameters decrease with the increase of the SCH thickness. The reason for the existence of the maximum value of the quantum well confinement factor Γ is that, as the thickness of the SCH increases, the light-restricting ability of the waveguide increases, and the mode field value of the waveguide at the quantum well increases. After reaching the highest point, the thickness of the SCH increases further. As a result, the mode field size increases, eventually resulting in a decrease in the field value of the mode at the quantum well. It should be pointed out that, unlike low-power communication laser chips, the design of high-power laser chips mainly considers whether the highest possible output power can be obtained, and the actual output power is limited by the highest power density that the bulk material and the facet coating can withstand. Therefore, in a high-power semiconductor laser design, the normalized power density value should be reduced as much as possible. In this paper, the normalized power density value is about 10 MW/cm^2.

光束发散角亦即远场分布与近场分布构成傅里叶变换关系,同时还需要考虑到光在半导体与空气界面处的光折射。图 2 ~ 图 4 为在对称波导情形时,波导层的铝组份分别比包层铝组份高

0.06、0.09 和 0.12 三种情况下的量子阱限制因子、光束发散角（半高全宽值:FWHM）、以及归一化功率密度与波导总厚度（SCH 层总厚度）之间的关系。在本论文中，归一化功率密度是指 100 μm条宽的有源区芯片输出功率为 10 W 时所对应的峰值功率密度。由图可见，3 个参量均在某一 SCH 厚度处取得最高值，过了最高点后，上述参量随 SCH 厚度的增加而减小。量子阱限制因子 Γ 存在最大值的原因在于:随着 SCH 厚度的增加，波导对光的限制能力随之增强，在量子阱处的波导模场值增大，当达到最高点后，SCH 厚度的进一步增加，导致了模场尺寸的增大，从而导致了量子阱处的模式的场值的减小。需要指出的是，不同于低功率通讯激光芯片，高功率激光芯片设计的主要考虑在于获得尽可能高的输出功率，而实际的输出功率受芯片材料以及腔面镀膜材料所能承受的最高功率密度限制，所以实际上在高功率半导体激光设计中，应尽可能降低归一化的功率密度值。在我们的设计中我们取归一化功率密度值为 10 MW/cm^{2}左右。

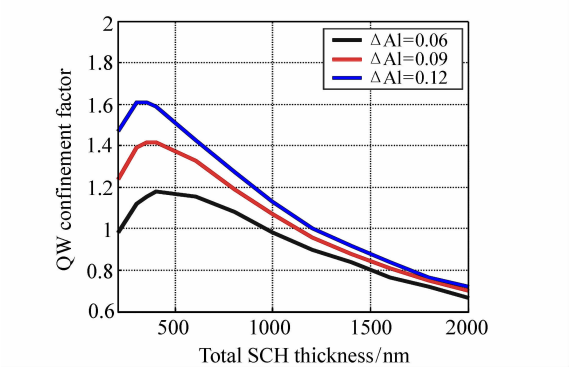

Fig. 2 Quantum well confinement factor versus total SCH thickness

图 2 量子阱限制因子与 SCH 总厚度之间的关系

It should be noted that Fig. 2 – Fig. 4 are calculated for symmetric waveguides. In order to increase the efficiency of the device as much as possible, we adopt a dual asymmetrical waveguide design based on the calculation of symmetric waveguides, that is: 1) the aluminum composition of the P-type AlGaAs material is higher than that of the N-type AlGaAs material; 2) the quantum well is placed asymmetrically in the SCH waveguide as shown in Fig. 5.

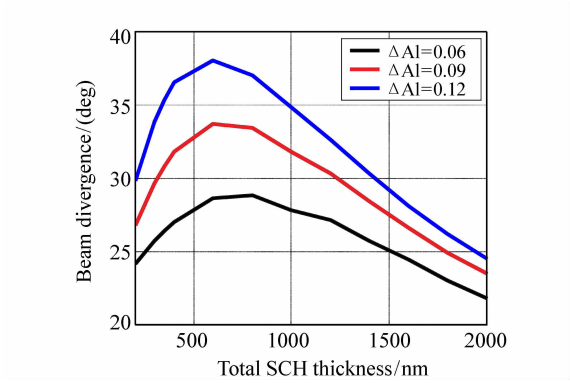

Fig. 3 Beam divergence (FWHM) versus total SCH thickness

图 3 光束发散角(FWHM)与 SCH 厚度之间的关系

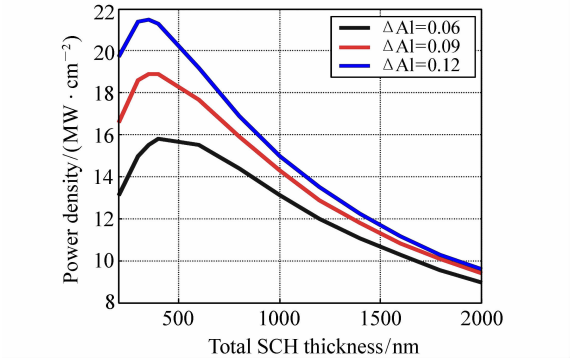

Fig. 4 Normalized power density versus total SCH thickness

图 4 归一化的功率密度与 SCH 厚度之间的关系

Fig. 5 – Fig. 6 show the calculated waveguide near-field and far-field distributions. From the near-field distribution, it can be seen that about 72% of the light field is on the side of the N-type region. The asymmetrical distribution of the light field allows us to simultaneously reduce internal losses and electrical resistance to a minimum. This is because considering light absorption, the cross-section of electrons is only about half of that of holes, and the mobility of electrons in Al(x)GaAs(when $x < 0.45$) is much higher than that of holes.

需要指出的是，图 2 ~ 图 4 是针对对称波导进行计算的。为了尽可能提高器件的效率，我们在对称波导计算的基础上，采用了双非对称波导设计:即(1)P 型 AlGaAs 材料的铝组份比 N 型 AlGaAs 材料的铝组份要高一些;(2)量子阱在

SCH 波导中是非对称的放置,如图 5 所示。图 5 ~ 图 6 给出了计算的波导近场与远场分布。从近场分布可以看出,大约 72% 的光场处于 N 型区域一边。光场的非对称分布使得我们能够同时将腔内损耗以及芯片电阻降低到最小程度。这是因为,电子对光的吸收截面大约只有空穴对光的吸收截面的一半左右,另外,电子在 Al(x)GaAs 材料中(当 x <0.45)的迁移率要远远高于空穴的迁移率。

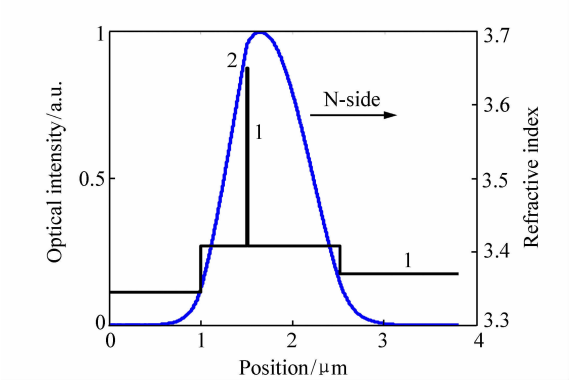

Fig. 5　Double unsymmetrical waveguide structure (line 1) and corresponding light field distribution (line 2)

图 5　双非对称波导结构(线 1)以及对应的光场分布(线 2)

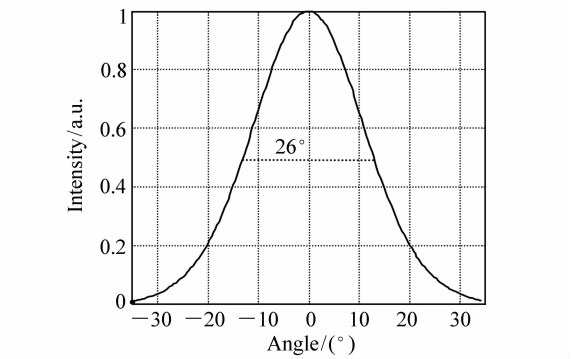

Fig. 6　Profile of far-field distribution

图 6　远场分布计算结果

After optimization of the waveguide, doping optimization should be considered because doping not only affects the series resistance of the chip but also affects the optical loss of the laser resonator. For shallowly etched waveguide, the scattering loss of the light at the material interface is negligible, so that the internal optical loss is completely determined by the absorption of free carriers and that of holes in the valence band transition. This means that as long as electrons and holes exist within the scope of the light field, absorption by the above mechanism will occur. Thus, the optical loss of the semiconductor laser is composed of three parts: one is the light absorption caused by electrons and holes in the quantum well, because the carrier concentration in the quantum well generally exceeds 1×10^{18} cm^{-3} during normal operation of the device; the second is the electron-induced absorption of light in the n-type region; the third is the light absorption caused by holes in the p-type doped region. Therefore, the total light loss and the resistance per unit area of the material and doping distribution can be expressed as:

波导优化完毕之后,随后的设计考虑是掺杂优化,因为掺杂不仅影响芯片的串联电阻,而且也影响激光谐振腔的光损耗。在波导为浅刻蚀情形下,光在材料界面处的散射损耗可以忽略不计,从而腔内的光损耗完全取决于自由载流子吸收以及空穴在价带间跃迁引起的吸收,这就意味着在光场所及的范围内,只要存在电子与空穴,上述机理引起的吸收就会发生。基于上述理由,半导体激光器的光损耗由三部分组成:其一为量子阱内的电子与空穴引起的光吸收,因为在器件正常工作时,量子阱内的载流子浓度一般会超过 1×10^{18} cm^{-3};其二为 n 型区域的电子引起的光吸收;其三为 p 型掺杂区域内的空穴引起的光吸收。所以,光的总损耗以及材料的单位面积电阻与掺杂分布可表示为:

$$\alpha = (C_{\mathrm{fc}} + C_{\mathrm{ivba}})\Gamma N_{\mathrm{th}} + C_{\mathrm{fc}} \int_{\text{n-side}} I(x) N_{\mathrm{d}}(x)\,\mathrm{d}x + C_{\mathrm{ovba}} \int_{\text{p-side}} I(x) N_{\mathrm{a}}(x)\,\mathrm{d}x\ , \tag{5}$$

$$R_0 = \int \frac{\mathrm{d}x}{e\mu_{\mathrm{e}} N_{\mathrm{d}}} + \int \frac{\mathrm{d}x}{e\mu_{\mathrm{h}} N_{\mathrm{a}}}\ , \tag{6}$$

Where Γ is quantum well confinement factor, N_{th} is the carrier concentration in the quantum well when the device reaches the threshold, $I(x)$ (the dimension is cm^{-1}) is a normalized light field distribution

whose integral over the entire growth direction is 1, indicating that the intensity distribution of the light field in the material growth direction, which is proportional to the square of the field strength E, and the field strength can be obtained by solving the aforementioned equation (1). C_{fc}, C_{ivba} (in cm^2) are the absorption cross-sections of the free carriers electrons and holes, respectively, N_d, N_a are the doping concentration distributions of donor and acceptor atoms, μ_e, μ_h are the mobility of electrons and holes in the material, e is the electron charge. In equation (5), the first term indicates light absorption due to carriers in the quantum well, and the second and third terms are the optical losses in the n-type doped region and the p-type doped region, respectively. In equation (6), the first and second terms are the resistances of the n-type region and the p-type region, respectively. The actual calculations show that for a 915 nm high-power laser structure using a large optical cavity, the light loss caused by the doping of the epitaxial layer can be reduced to below 0.2/cm through doping optimization, and the resistance per unit area of the device can be reduced to below 6.0×10^{-5} $\Omega\cdot cm^2$.

式中,Γ 为量子阱限制因子,N_{th}为器件达到阈值时量子阱内的载流子浓度,$I(x)$(量纲为 cm^{-1})是归一化的光场分布,其在整个生长方向上的积分为1,表示光场在材料生长方向上的强度分布,与场强 E 的平方成正比,而场强可以由求解前述的方程(1)而得到。C_{fc}、C_{ivba}(单位为 cm^2)分别为自由载流子电子与空穴的吸收截面,N_d、N_a分别为施主与受主原子的掺杂浓度分布,μ_e、μ_h 分别为电子与空穴在材料中的迁移率,e 为电子电荷量。在(5)式中,第一项表示量子阱内的载流子引起的光吸收,第二与第三项分别为 n 型掺杂区域与 p 型掺杂区域内的光损耗。在式(6)中,第一与第二项分别是 n 型区域与 p 型区域的电阻。实际计算表明,对于采用大光腔的915 nm 高功率激光结构,经过掺杂优化,外延层掺杂引起的光损耗 α 可以减小到 0.2/cm 以下,同时器件的单位面积电阻可以降低到 6.0×10^{-5} $\Omega\cdot cm^2$以下。

Appropriate cavity length for the required output power is to be calculated by device design. Careful consideration has been given to thermal issues during packaging for cavity length calculations. A three-dimensional numerical analysis method is adopted to analyze the heat dissipation typically used for packaging of 915 nm fiber laser pump modules to calculate the thermal resistance of the entire package module. The calculation assumes that the chip's electrical injection region has a width of 95 μm and is soldered to the AlN heat sink with a thickness of 350 μm (this type of package is called COS) in the form of P-face down. The AlN heat sink is then welded on a 2 mm thick copper block. Equations (7) and (8) give the relationship of the thermal resistance of the package module varies with the length of the laser cavity and the corresponding change in the junction temperature, respectively:

器件设计主要计算对于要求的输出功率时所需要的合适腔长。腔长计算时需要仔细考虑封装时的热问题。我们采用三维数值分析方法分析了典型的用于915 nm 光纤激光泵浦模块热封装的热场分布,从中计算出整个封装模块的热阻。在计算中,假定芯片的电注入区宽度为95 μm 并以P面朝下的形式被焊接在厚度为350 μm 的 AlN 热沉上(这一封装形式被称之为 COS),随后 AlN 热沉再被焊接在2 mm 厚的铜块上。式(7)与式(8)分别给出了上述封装模块的热阻随激光器腔长的变化关系以及对应的结温变化:

$$R_t = \frac{0.96}{L+0.03}, \tag{7}$$

$$\Delta T = R_t Q, \tag{8}$$

where L is the cavity length of the laser which is given in centimeters. The dimension of the thermal resistance is K/W, Q is the thermal power (in Watt) generated by the chip. ΔT is the chip junction temperature rises, which is given in K. After the high-power laser is fabricated, the facets are coated as required. The reflectivity of the rear facet coating is usually greater than 95%. The reflectivity of the front facet coating (*i. e.*, the light exiting facet) is opti-

mized based on the epitaxial structure, device cavity length, and light output power. This is because the reflectance affects both the device′s threshold current and the external quantum efficiency. Using the self-developed semiconductor laser design software, the dependences of device′s electro-optical conversion efficiency (WPE) and the output power on the device cavity length and front-facet reflectivity at an injected current of 12 A and at room temperature at 25 ℃ are calculated (see Fig. 7 – Fig. 8). In this calculation model, the calculations to be performed include: discrete energy levels in quantum well structures and their corresponding quantum wells, material gain and spontaneous emission coefficient, optical waveguide and its quantum well limiting factor, and heat dissipation of packaged modules and corresponding thermal resistance, light-current-voltage (L-I-V) characteristics, *etc*. From the simulation results, it can be seen that the electro-optical conversion efficiency at a cavity length of 4.8 mm reaches 67% when the AR film reflectivity is about 1%, and the output power exceeds 13 W. In the case of the fixed front-facet reflectance, due to the interaction between the parameters of mirror loss, electrical resistance and thermal resistance, the output power will decreases as the cavity length increases, while the electro-optical conversion efficiency increases as the cavity length increases.

式中，L 为激光器的腔长，单位为厘米，热阻的量纲为 K/W，Q 为芯片产生的热功率，单位为瓦，ΔT 为芯片结温升高量，单位为 K。高功率激光器制作完毕后，需要根据需要对腔面进行镀膜处理，后腔面的反射率通常大于 95%，而前腔面（即出光面）的反射率需要根据外延结构、器件腔长以及出光功率大小进行优化。这是因为腔面反射率会同时影响器件的阈值电流以及外量子效率。利用我们自己研发出的半导体激光器设计软件，我们计算了器件在 25 ℃室温下，当注入电流为12 A时的电光转换效率（WPE）以及输出功率与前腔面抗反射膜（antireflection coating）反射率和腔长之间的关系（见图 7，图 8）。在我们的计算模型中，所需要进行的计算包括：量子阱结构及其对应的量子阱内的分立能级计算，材料增益以及自发辐射系数计算、光波导及其量子阱限制因子计算、封装模块的热分析及其对应的热阻计算，光—电流—电压（L-I-V）特性计算等。由仿真计算可以看出，腔长为 4.8 mm 时的电光转换效率在 AR 膜反射率为 1% 左右时达到 67%，而输出功率超过 13 W。在相同 AR 膜反射率情况下，因为腔面光提取效率、电阻以及热阻等参量之间的相互作用，导致输出功率随腔长增加而减小，而电光转换效率却随腔长增加而增大。

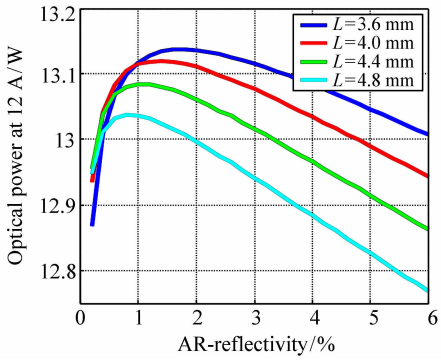

Fig. 7　Relationship between output power, cavity length and reflectivity of antireflection (AR) layer

图 7　输出功率与腔长以及 AR 膜反射率之间的关系

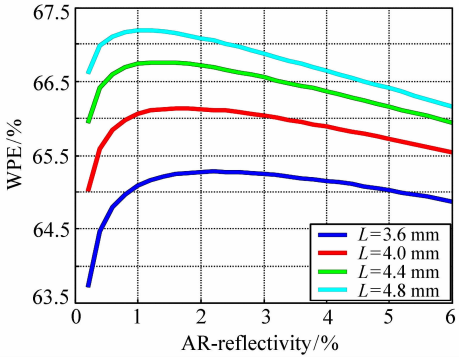

Fig. 8　Relationship between electro-optical conversion efficiency, cavity length, and reflectivity of antireflection (AR) layer

图 8　电光转换效率与腔长以及 AR 膜反射率之间的关系

3 Material growth, process production and testing
材料生长,器件制作与测试

The epitaxial material is grown by metal organic vapor deposition(MOCVD). The quantum well is an $In_{0.10}GaAs$ with a thickness of about 7 nm and the barrier is an $Al_{0.23}GaAs$ material. The thickness of the entire SCH layer is 1.5 μm. The device process begins with the definition of the waveguide by optical exposure, followed by electrical contact windows, P-side metallization, wafer thinning, N-side metallization, rapid annealing, facet passivation and coating etc. In order to enable the device to operate as a continuous wave at high currents, we soldered the device on a 350 μm thick AlN ceramic with P side down, and 30 gold wires are welded on the N side. Fig. 9 is a photo-current (LI) characteristic curve and a corresponding electro-optical conversion efficiency curve measured at a continuous current mode (CW) at a temperature of 20 ℃, which consists of the proportion of the threshold current in the overall injected current, the Joule heating, and the thermal, optical, and electrical interactions. It can be seen that, at 20 ℃, the COS threshold current is about 1 A, the slope efficiency is about 1.18 W/A, and the operating current required to reach 12 W output power is 11.5 A. The highest electro-optic conversion efficiency is 66.5%. When the output power is 12 W, the electro-optical conversion efficiency is reduced to 64.3%. The above test results are in good agreement with the simulation in Fig. 7 – Fig. 8, which shows that this design software can accurately predict the performance of the device. In order to find the facet damage threshold of the device, a destructive test on the device under high current is conducted. The test conditions are 20 ℃ quasi-continuous-wave(QCW) current mode and 40 ℃ continuous current mode. In the QCW test, the pulse width is 1 ms and the repetition rate is 1 KHz. During the test, the current increase continuously until the sudden loss of power due to facet damage. The test results are shown in Fig. 10. As can be seen from Fig. 10, the facet COD power value is 23.8 W under the QCW condition, and the facet damage threshold power becomes 18.1 W during the CW test. Fig. 11 shows the relationship between the divergence angle of the beam and the injected current when the energy contained in the beam is 95% of the total energy. It can be seen from the figure that in the process of increasing the current from 2 A to 12 A, the far field in the vertical direction remains basically constant. However, the horizontal far field increases with the increase of the current. This change is related to various mechanisms, including the thermal lens effect and the spatial hole burning effect of carriers. Since the reliability of lasers is critical for industrial applications, we have performed life testing of COS devices under over-current conditions[18]. The test conditions are as follows: temperature 35 ℃, 14 A constant current. The output power is 14 W under this condition. Fig. 12 shows the recording of the power of the eight COS devices over time under the above test conditions. It is clear that the power of the device did not change during the life test of about 6 000 hours, indicating that our device works reliably even in high temperature(35 ℃) and high current(14 A) and high power(14 W).

外延材料用金属有机气相沉积(MOCVD)生长而成。量子阱为7 nm左右的$In_{0.10}GaAs$,而势垒为$Al_{0.23}GaAs$材料,整个SCH层的厚度为1.5 μm。器件工艺以光学曝光以定义波导为起点,随后有电接触窗口、P面金属化、晶片减薄、N面金属化、快速退火以及解理钝化与腔面镀膜等工序。为了使得器件能够在高电流下以连续波形式工作,我们将器件以P面朝下的方式焊接在350 μm厚的AlN陶瓷上,随后在N面打上30根金丝线。图9为在20 ℃温度下以持续电流方式(CW)测试的光—电流(L-I)特性曲线以及对应

的电光转换效率曲线,该典型效率曲线是由阈值电流在整体注入电流中的比例、焦耳热以及热、光、电相互作用构成的。由其可见,COS 在 20 ℃测试环境下,阈值电流大约为 1 A,斜率效率大约为 1.18 W/A,而达到 12 W 输出功率时所需要的工作电流为 11.5 A。电光转换效率最高值为 66.5%,当输出功率为 12 W 时,电光转换效率减小到为 64.3%,上述测试结果与图 7、图 8 的模拟结果非常吻合,说明我们的设计软件能够准确预测器件的性能。为了找出器件的腔面损伤阈值,我们对器件在高电流下进行了破坏性测试,测试条件分别为 20 ℃准持续(QCW)电流模式以及 40 ℃持续电流模式。在 QCW 测试时,脉宽为 1 ms,重复频率为 1 kHz。在测试过程中,电流持

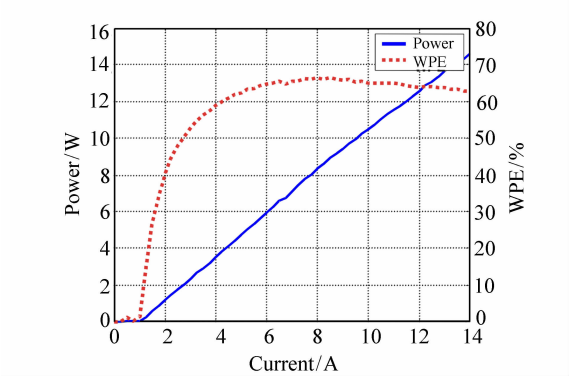

Fig. 9　Photocurrent curve and electro-optical conversion efficiency curve of 915 nm single-tube COS module at 20 ℃

图 9　915 nm 单管 COS 模块在 20 ℃下的光—电流曲线与电光转换效率曲线

续增加,直到因腔面损伤而功率急剧衰减为止。测试结果如图 10 所示。由图 10 可见,在 QCW 条件下,腔面 COD 功率值为 23.8 W,而在 CW 测试时,腔面损伤阈值功率则变为 18.1 W。图 11 为光束所含能量为总能量的 95% 时所对应的光束发散角与注入电流的关系,由图 11 可见,垂直方向的远场在电流从 2 A 增到 12 A 过程中,基本维持恒定,而水平远场则随电流的增大而增大,这一变化与多种机理有关,包括热透镜效应以及载流子的空间烧孔效应。鉴于激光器的可靠性对工业应用来说至关重要,我们对 COS 器件进行了过电流条件下的寿命测试[18],测试条件为:温度 35 ℃,14 A 恒定电流。在该条件下,输出功率为

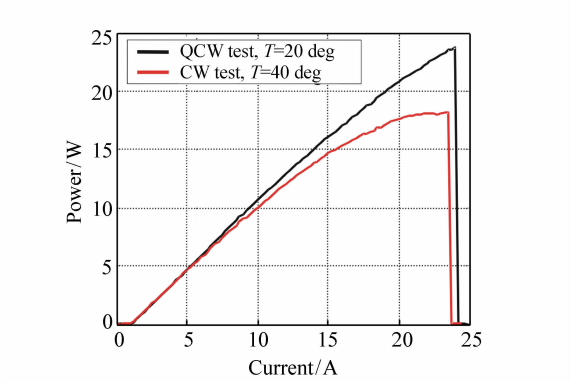

Fig. 10　Cavity damage power tested under quasi-continuous(QCW) and continuous(CW) conditions

图 10　在准持续(QCW)以及持续(CW)条件下测试的腔面损伤功率

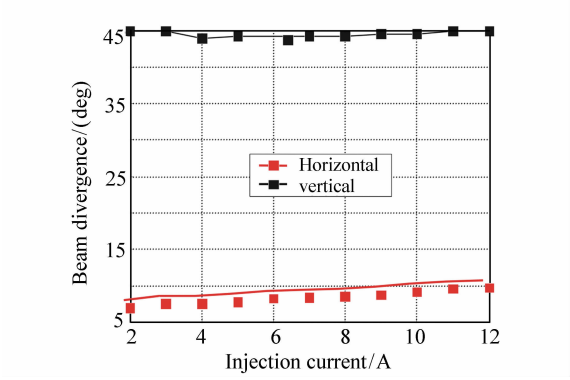

Fig. 11　Beam divergence angle corresponding to 95% of the total energy

图 11　95% 能量所对应的光束发散角值

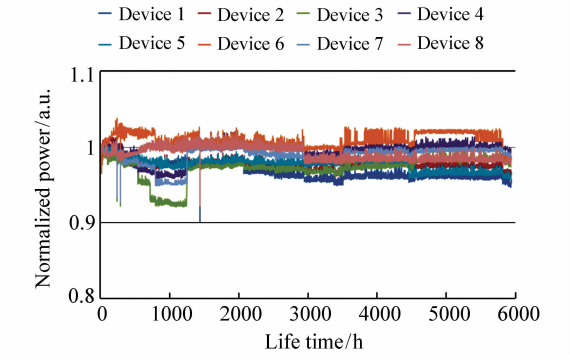

Fig. 12　Life test record(device initial power 14 W, test temperature 35 ℃, current 14 A)(colour figures is availabe in electro-version)

图 12　寿命测试记录(器件初始功率为 14 W,测试温度为 35 ℃,电流为 14 A)(见彩图)

14 W。图12为8个COS器件在上述测试条件下的功率随时间变化的记录,很显然在大约6 000 h的寿命测试过程中,器件的功率没有变化,说明我们的器件即使在高温环境(35 ℃)以及高电流(14 A)和高功率(14 W)时依然能够可靠工作。

4 Conclusion
结 论

This paper briefly describes the design, fabrication, and testing results of high power 915 nm semiconductor laser manufactured by Shenzhen Raybow Optoelectronics Co., Ltd. The test results show that the electro-optical conversion efficiency of the developed device is up to 66.5%, and the electro-optical conversion efficiency can still reach 64.3% when the output power is 12 W. This efficiency has reached the advanced level of similar devices in the world. Under the accelerated life test conditions of 35 ℃ and 14 A injection current (corresponding to output power of 14 W), the output power of the device remained stable during the test period of about 6 000 hours, indicating that the reliability of the device is satisfactory.

本文简要叙述了瑞波光电子公司的高功率915 nm半导体激光的设计、制作与测试结果。测试结果表明,研发的器件电光转换效率最高达66.5%,输出功率为12 W时的电光转换效率仍然达到64.3%,这一效率指标达到国际同类器件的先进水平。在35 ℃、14 A注入电流(对应输出功率14 W)的加速寿命测试条件下,器件的输出功率在大约6 000 h的测试过程中保持稳定,说明器件的可靠性令人满意。

参考文献:

[1] STILES E. New developments in IPG fiber laser technology[C]. Proceedings of the 5th International Workshop on Fiber Lasers, Dresden, Germany, 2009.

[2] VAISSIE L, STEELE T, RUDY P. High-power diode lasers advance pumping applications[J]. *Laser Focus World*, 2008, 44(6).

[3] FAIRCLOTH B O. High-brightness high-power fiber coupled diode laser system for material processing and laser pumping [J]. *Proceedings of the SPIE*, 2003, 4973: 34-41.

[4] 王鑫, 赵懿昊, 王翠鸾, 等. 110 W高功率高亮度915 nm半导体激光器光纤耦合模块研究[J]. 发光学报, 2017, 38(12): 1654-1660.
WANG X, ZHAO Y H, WANG C L, *et al*.. 110 W high power and high brightness 915 nm fiber coupled laser diode module[J]. *Chinese Journal of Luminescence*, 2017, 38(12): 1654-1660. (in Chinese)

[5] 王立军, 宁永强, 秦莉, 等. 大功率半导体激光器研究进展[J]. 发光学报, 2015, 36(1): 1-19.
WANG L J, NING Y Q, QIN L, *et al*.. Development of high power diode laser[J]. *Chinese Journal of Luminescence*, 2015, 36(1): 1-19. (in Chinese)

[6] MORITA T, NAGAKURA T, TORII K, *et al*.. High-efficient and reliable broad-area laser diodes with a window structure [J]. *IEEE Journal of Selected Topics in Quantum Electronics*, 2013, 19(4): 1502104.

[7] CRUMP P, BLUME G, PASCHKE K, *et al*.. 20 W continuous wave reliable operation of 980 nm broad-area single emitter diode lasers with an aperture of 96 μm[J]. *Proceedings of the SPIE*, 2009, 7198: 719814.

[8] SCHULTZ C M, CRUMP P, WENZEL H, *et al*.. 11 W broad area 976 nm DFB laser with 58% power conversion efficiency [J]. *Electronics Letters*, 2010, 46(8): 580-581.

[9] CRUMP P, SCHULTZ C, PIETRZAK A, *et al*.. 975-nm high-power broad area diode lasers optimized for narrow spectral linewidth applications[J]. *Processongs of SPIE*, 2010, 7583: 75830N-10.

[10] PETRESCU-PRAHOVA I B, MODAK P, GOUTAIN E, *et al*.. High d/gamma values in diode laser structures for very high power[J]. *Proceedings of the SPIE*, 2009, 7198: 71981I-8.

[11] LOYO-MALDONADO V, BACCHIN G, ROBERTSON S, *et al*.. High reliability operation of 2 kW QCW 10-bar laser diode stacks at 808 nm[J]. *Proc. of SPIE*, 2009, 7198: 71981E-8.

[12] KNAUER A, ERBERT G, STASKE R, *et al*.. High-power 808 nm lasers with a super-large optical cavity[J]. *Semicon-*

ductor Science and Technology,2005,20(6):621-624.

[13] AVRUTIN E A.,RYYKIN B S. Thery and modelling of the power conversion efficiency of large optical cavity laser diodes[C]. 2015 High power diode lasers and systems conference(HPD),IEEE,Coventry,UK,2015:9-10.

[14] QIU B C,MCDOUGALL S D,LIU X F,*et al*.. Design and fabrication of low beam divergence and high kink-free power lasers[J]. *IEEE Journal of Quantum Electronics*,2005,41(9):1124-1130.

[15] TSAI C Y,TSAI CH Y,CHEN C H,*et al*.. Theoretical model for intravalley and intervalley free-carrier absorption in semiconductor lasers: beyond the classical drude models[J]. *IEEE Journal of Quantum Electronics*,1998,34(3):552-559.

[16] CHILD G N,BRAND S,ABRAM R A. Intervalence band absorption in semiconductor materials[J]. *Semiconductor Science and Technology*,1986,1:116-120.

[17] CHUANG S L. *Physics of Optoelectronic Devices*[M]. New York:John Wiley & Son Inc,1995.

[18] 王文知,井红旗,祁琼,等.大功率半导体激光器可靠性研究和失效分析[J].发光学报,2017,38(2):165-169.
WANG W Z,JJING H Q,QI Q,*et al*.. Reliability test and failure analysis of high power semicounductor laser[J]. *Chinese Journal of Luminescence*,2017,38(2):165-169.(in Chinese)

作者简介:

QIU Bo-cang (1962—) received his bachelor's degree in engineering from Xi'an Jiaotong University in 1983, a master's degree in engineering from Beijing Institute of Technology in 1986, and a doctor's degree from Glasgow University in England in 1998. He is currently a design expert for the Institute of High-end Semiconductor Laser Research of Shenzhen Tsinghua University and the design director of Shenzhen Raybow Optoelectronics Co., Ltd. He is mainly engaged in the research of semiconductor lasers. Dr. Qiu specializes in semiconductor optoelectronic devices, especially in semiconductor laser processes and designs. He has published 110 academic papers in the industry's top journals and academic conferences and applied for 14 invention patents. E-mail: qiubocang@raybowlaser.com

仇伯仓(1962—),男,陕西永寿县人,博士,研究员。1983 年于西安交通大学获工学学士学位,1986 年于北京理工大学获得工学硕士学位,1998 年于英国格拉斯哥大学获得博士学位。现为深圳清华大学研究院高端半导体激光器研究中心设计专家,深圳瑞波光电子有限公司设计总监,主要从事半导体激光器方面的研究,在行业内的顶级期刊与学术会议上共发表了 110 篇学术论文,申请了 14 项发明专利。E-mail: qiubocang@raybowlaser.com

BAI Xue(1987—) received her bachelor's degree from Henan University of Technology in 2009 and a master's degree from Henan University of Technology in 2012. She is currently a project engineer at Shenzhen Raybow Optoelectronics Co., Ltd. and is mainly engaged in the research of semiconductor lasers. E-mail: baixue@raybowlaser.com

白雪(1987—),女,山东莱芜人,硕士,工程师,2009 年、2012 年于河南工业大学分别获得学士、硕士学位,现为深圳瑞波光电子有限公司项目工程师,主要从事半导体激光器方面的研究。E-mail:baixue@raybowlaser.com